tems. Higher-order systems can be analyzed in a similar manner by defining a separate coupling parameter for every pair of subsystems.

A simple test structure consisting of a cantilever beam with attached disk has been used to experimentally verify the stability analysis. This structure exhibits bending and torsion at nearly the same frequency. The force actuators can be relocated so that the degree of coupling between bending and torsion can be easily adjusted. Initial condition responses on this structure for several coupling values confirm that the performance severely degrades as the degree of coupling approaches the critical value, where the system becomes unstable for both decentralized and centralized controllers. Thus, to ensure stable control, the actuators should be located so that the coupling they induce is sufficiently different from the critical value.

Acknowledgments

The research described in this document was made possible in part by funds from an NEC Fellowship to Peter H. Meckl, provided by NEC Corporation, Tokyo, Japan. We also gratefully acknowledge Haruo Shimosaka from Meiji University, Kawasaki, Japan, for helping with the design and analysis of the test structure.

References

[1]Sandell, N. R., Jr., Varaiya, P., Athans, M., and Safonov, M. G., "Survey of Decentralized Control Methods for Large Scale Systems," *IEEE Transactions on Automatic Control,* Vol. AC-23, No. 2, 1978, pp. 108–128.

[2]Wang, S.-H., and Davison, E. J., "On the Stabilization of Decentralized Control Systems," *IEEE Transactions on Automatic Control,* Vol. AC-18, No. 5, 1973, pp. 473–478.

[3]Nwokah, O. D. I., and Perez, R. A., "On Multivariable Stability in the Gain Space," *Automatica,* Vol. 27, No. 6, 1991, pp. 975–983.

[4]Iftar, A., and Özgüner, Ü., "Local LQG/LTR Controller Design for Decentralized Systems," *IEEE Transactions on Automatic Control,* Vol. AC-32, No. 10, 1987, pp. 926–930.

[5]Horner, J. B., Meckl, P., and Shimosaka, H., "Modeling and Design of a Structure for Decentralized Active Vibration Control," *Active Noise and Vibration Control—1990,* ASME NCA-Vol. 8, ASME Winter Annual Meeting, Dallas, TX, 1990, pp. 153–159.

Design of Robust Quantitative Feedback Theory Controllers for Pitch Attitude Hold Systems

David E. Bossert*
U.S. Air Force Academy, Colorado 80840

Introduction

THE importance of robust controllers is seen by their application to situations involving plant or transfer function uncertainty. Plant uncertainty can arise from variations in plant dynamics throughout a performance range or from the inability to accurately model a complicated plant. Quantitative Feedback Theory (QFT) is one technique which has proven useful in robust control applications. QFT is a unified theory that emphasizes the use of feedback for achieving the desired system performance tolerances despite plant uncertainty and plant disturbances.[1]

Received May 18, 1992; presented as Paper 92-4409 at the AIAA Guidance, Navigation, and Control Conference, Hilton Head, SC, Aug. 10–12, 1992; revision received Oct. 25, 1992; accepted for publication March 12, 1992. This paper is declared a work of the U.S. Government and is not subject to copyright protection in the United States.

*Assistant Professor, Department of Aeronautics. Member AIAA.

QFT compares favorably to other robust techniques such as H-infinity.[2] Application to stable and unstable plants as well as linear and nonlinear plants shows the versatility of the technique.[3,4] Specific applications have ranged from flight control problems[5] to PUMA-560 robotic manipulators.[6–8] Aircraft transfer functions vary with flight conditions such as speed and altitude and provide a good challenge for robust control techniques.[9]

As case studies, a business jet and an F-4 fighter jet provide an interesting comparison for the application. The dynamics for three flight conditions cause a wide range of parameter uncertainties to arise. Additionally, inclusion of a fast and a slow actuator demonstrates the actuator's effect on the performance of the aircraft.[9] The slower actuator may represent any additional lags in the system which serve to degrade aircraft performance.

The model development section details the flight conditions used to derive the plant cases. Then, military standard MIL-F-8785B provides the guidance for the development of flight performance specifications for all categories of flight. The fourth section provides a mathematical validation of the design and the fifth section provides some insight into design tradeoffs. Finally, the last section presents the conclusion.

Model Development

Aircraft dynamics change with flight conditions, and this causes flight uncertainty throughout a typical mission. For the business jet case study, three flight conditions represent the uncertainty for a flight in this test case.[9] Flight condition 1 displays the low-speed dynamics associated with landing, while flight conditions 2 and 3 exhibit high-speed subsonic cruise dynamics. Condition 2 also shows the effect of increased moment of inertia on the aircraft dynamics. A short period approximation[9] is used for the models.

Aircraft normally incorporate actuators to make required stick forces manageable for control surface deflections, especially at high dynamic pressures.[9] However, actuators contribute lag to the aircraft system. Therefore, a designer must account for these delays. To represent additional unmodeled delays in the system, two actuators are used. One has a time constant of 0.08 s and an additional actuator is modeled with a time constant of 0.10 s.

Combining three transfer functions with two actuators yields a total of six plants. These plants represent parameter uncertainty based on speed, altitude, weight, and system lag. The maximum variation is 15.787 dB between the different plants. This case study gives a representative problem for the application of QFT.

An F-4 fighter jet provides the dynamics for the second case study. The F-4 is substantially different from a business jet, in particular because of its supersonic capabilities. Flight conditions include power approach, subsonic cruise, and supersonic cruise. The aircraft dynamics vary greatly over this range of flight conditions. Table 1 lists the plants for both the business jet and the fighter jet.

Flight Performance Specifications

The most restrictive requirements are for category A in military standard MIL-F-87875B. Choosing the most restrictive ζ and ω_n results in a range of $0.932 \text{ s} < Ts_{2\%} < 4.57$ s for the business jet and $0.735 \text{ s} < Ts_{2\%} < 4.16$ s. The maximum peak for both cases, based on $\zeta_{\min}$ is 1.309.

Quantitative Feedback Theory Design

Several sources[1,3] provide the details of the QFT design procedure. The results of this design are presented here rather than the details due to space limitations. The tracking specifications developed from MIL-F-8785B serve as the tracking bounds, and the disturbance bound is arbitrarily chosen as -20 dB at all frequencies. Figure 1 shows the nominal loop transmissions that satisfy the tracking and disturbance bounds for both the business jet and the fighter jet. This results in the

following controller for the business jet:

$$G(s) = \frac{5.542 \times 10^9 (s + 0.1)(s + 3.5)(s + 6)(s + 15)}{s(s + 0.7)(s + 400)(s + 2100 \pm j2142.4)} \quad (1)$$

and the following controller for the fighter jet:

$$G(s) = \frac{9.337 \times 10^8 (s + 3.5)(s + 6)(s + 7)}{s(s + 400)(s + 1061 \pm j1061)} \quad (2)$$

Filters help shape the desired response of the controller. To show the flexibility of shaping the response, filters which yield an underdamped response and an overdamped response are given for both jets. For both the business and fighter jets, the overdamped filter is

$$F(s) = 0.20(s + 20)/[(s + 1)(s + 4)] \quad (3)$$

and the underdamped filter is

$$F(s) = 0.20(s + 20)/(s + 1 \pm j1.732) \quad (4)$$

Validation

Validating the design requires entering a step input into the tracking and disturbance inputs for each plant condition to verify that each plant meets specifications. All cases met tracking and disturbances specifications for both case studies. Figure 2 shows the frequency response of the business jet with an underdamped filter falls within the tracking bounds. The time response of the fighter jet with the overdamped filter falls within the tracking bounds in Fig. 3.

Insights

This design considered six cases and three flight conditions for two distinctly different aircraft. If the models are correct, then the design should work on the physical aircraft. However, the design did not consider actuator saturation in the model. Therefore, some adjustments in the gain might have to be made during the tuning process. Also, pilot inputs would require fine tuning of the controllers as well. Additionally, lag in excess of that modeled by the actuators might effect the system. For example, if a large sample time is present or the actuators are slower than modeled, the actuator authority might be exceeded since the error signal would become too large. This is a problem common to high-gain controllers in general.

Table 1 Jet plant sets

Plant	Transfer function (bus jet)
1	$P1(s) = \frac{37.8894(s + 0.5812)}{s(s + 12.5)(s + 0.89655 \pm j1.3319)}$
2	$P2(s) = \frac{30.3115(s + 0.5812)}{s(s + 10)(s + 0.89655 \pm j1.3319)}$
3	$P3(s) = \frac{178.5(s + 0.6395)}{s(s + 12.5)(s + 0.9945 \pm j2.6480)}$
4	$P4(s) = \frac{142.8(s + 0.6395)}{s(s + 10)(s + 0.9945 \pm j2.6480)}$
5	$P5(s) = \frac{188.5163(s + 0.9222)}{s(s + 1.5)(s + 1.1795 \pm j2.7551)}$
6	$P6(s) = \frac{150.813(s + 0.9222)}{s(s + 10)(s + 1.1795 \pm j2.7551)}$
Plant	**Transfer function (fighter jet)**
1	$P1(s) = \frac{18.2078(s + 0.4125)}{s(s + 12.5)(s + 0.4436 \pm 0.6174)}$
2	$P2(s) = \frac{14.5663(s + 0.4125)}{s(s + 10)(s + 0.4436 \pm j0.6174)}$
3	$P3(s) = \frac{142.49(s + 0.4965)}{s(s + 12.5)(s + 0.6269 \pm j2.7816)}$
4	$P4(s) = \frac{113.99(s + 0.4965)}{s(s + 10)(s + 0.6269 \pm j2.7816)}$
5	$P5(s) = \frac{143.53(s + 0.2552)}{s(s + 12.5)(s + 0.3118 \pm j4.8538)}$
6	$P6(s) = \frac{114.82(s + 0.2552)}{s(s + 10)(s + 0.3118 \pm j4.8538)}$

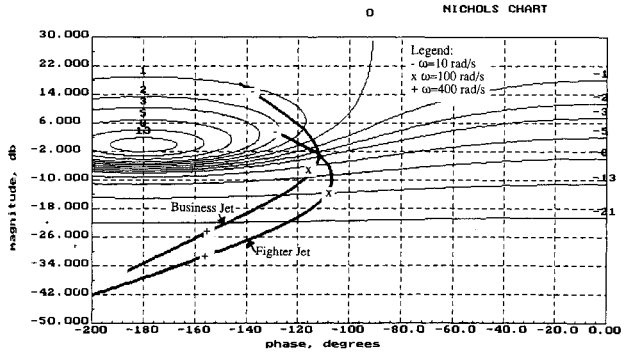

Fig. 1 Nominal loop transmissions.

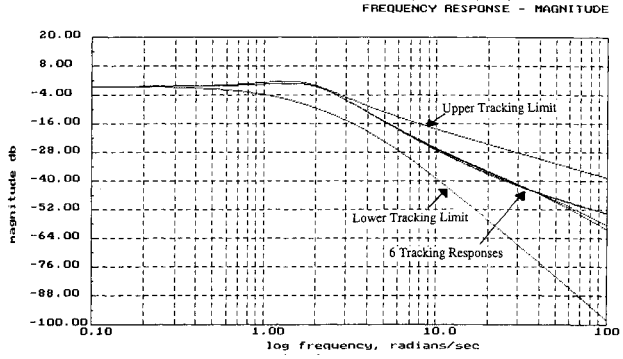

Fig. 2 Business jet underdamped frequency response.

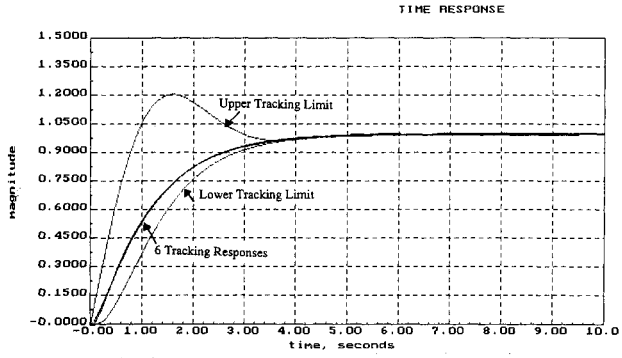

Fig. 3 Fighter jet overdamped time response.

Conclusion

The QFT technique is successfully applied to three flight conditions and two actuators for both a business jet and a fighter jet. Actual flight parameters provide the data for the aircraft plants, which include a fast and slow actuator. Time specifications developed from MIL-F-8785B are applied as the basis for the QFT design. Mathematically inputting step tracking and disturbance inputs validates the QFT design. The results show all flight condition/actuator combinations meet desired tracking and disturbance specifications.

References

[1]D'Azzo, J., and Houpis, C., *Linear Control System Analysis and Design,* McGraw-Hill, New York, 1988, pp. 686-742.

[2]Chait, Y., and Hollot, C., "A Comparison Between *H*-Infinity

Methods and QFT for a SISO Plant with Both Plant Uncertainty and Performance Specifications," *1990 ASME Winter Annual Meeting,* DSC-Vol. 24, ASME, New York, 1990, pp. 33-39.

[3]Horowitz, I., and Breiner, M., "Quantitative Synthesis of Feedback Systems with Uncertain Nonlinear Multivariable Plants," *International Journal of Systems Science,* Vol. 12, 1981, pp. 563-593.

[4]Horowitz, I., "Quantitative Feedback Theory," *IEEE Proceedings on Control Theory and Applications,* Vol. 29, 1982, pp. 215-216.

[5]Horowitz, I., "Application of Quantitative Feedback Theory (QFT) to Flight Control Problems," *Proceedings of the 1990 IEEE Conference on Decision and Control,* 1990, pp. 2593-2598.

[6]Bossert, D., "Design of the Pseudo-Continuous Time Quantitative Feedback Theory Robot Controllers," M.S. Thesis, Dept. of Electrical Engineering, AFIT/GE/ENG/89D-2.

[7]Bossert, D., Lamont, G., Leahy, M., Jr., and Horowitz, I., "Model-Based Control with QFT," *Proceedings of the IEEE International Conference on Robotics and Automation,* 1990, pp. 2058-2063.

[8]Leahy, M., Bossert, D., and Whalen, P., "Robust Model-Based Control: An Experimental Case Study," *Proceedings of the IEEE International Conference on Robotics and Automation,* 1990, pp. 1982-1987.

[9]Roskam, J., *Airplane Flight Dynamics and Automatic Flight Controls, Part 1,* Roskam Aviation and Engineering Corp., Ottawa, KS, 1979, pp. 412-444, 598-633.

Determining the Root Locations of Systems with Real Parameter Perturbations

Shyi-Kae Yang* and Chieh-Li Chen†
National Cheng-Kung University,
Tainan, Taiwan 70101, Republic of China

Introduction

THE problem of robust stabilization and control of interval systems has received widespread interest since the introduction of Kharitonov's theorem[1,2] and several extensions.[3-5] Recently, the problem of the robust root locus has been considered by Barmish and Tempo.[6] However, their work was limited to the case where the coefficients of the characteristic polynomial are linear affine functions of physical parameters.

In this Note, an alternative algorithm for checking the zero inclusion condition of an interval system, where the coefficients of its characteristic polynomial are multilinear affine functions of physical parameters, is proposed. Use of the algorithm for determining the robust root locations is presented. Numerical examples are given to illustrate the effectiveness of the proposed approach.

Preliminary Definitions

Let the closed-loop characteristic polynomial of an interval system be described as

$$\Delta(s, q, K) = s^m + \sum_{i=0}^{m-1} \delta_i(q, K)s^i \tag{1}$$

where K is the loop gain, $q \in Q \subset R^\ell$ denotes a vector of physical parameters with $Q = \{q | q_i \in [q_i^-, q_i^+], i = 1, \ldots, \ell\}$ and $\delta_i(q, K)$ are multilinear affine functions of q.

Definition 1: A point $\beta \in C$ located inside a convex polygon, conv(P), is said to satisfy the point inclusion condition (PIC) with respect to conv(P) and is denoted as

$$\beta \in \text{conv}(P) \tag{2}$$

where conv(P) is the convex polygon consisting of a set of points P.

Proposition 1: A point β satisfies the PIC with respect to conv(P) if and only if the area of conv(P) is equal to the area of conv($\{p_i | p_i \in P \cup \beta\}$).

If β is chosen to be the origin of the complex plane, the zero inclusion condition[6] (ZIC) can be restated as follows.

Corollary 1: The ZIC with respect to conv(P) is satisfied if and only if

$$\text{area}[\text{conv}(P)] = \text{area}[\text{conv}(\{p_i | p_i \in P \cup (0, 0)\})] \tag{3}$$

where area[conv($\cdot$)] denotes the area of conv($\cdot$) and P represents the images of the hypercube's vertices in the physical parameter space.

The image of linear affine (LA) mappings, LA($\cdot$), has the following feature.

$$\text{LA}(Q) = \text{LA}\{\text{conv}[\text{vert}(Q)]\} = \text{conv}\{\text{LA}[\text{vert}(Q)]\} \tag{4}$$

where vert(Q) is the set of the vertices of Q. For the multilinear affine (MLA) mapping, MLA($\cdot$), it satisfies that

$$\text{MLA}(Q) \subset \text{conv}\{\text{MLA}[\text{vert}(Q)]\} \tag{5}$$

Partition Q into p^{n-1} subdomains Q_i by partitioning each q_j, $j \neq k$, into p segments, i.e.,

$$Q = \bigcup_{i=1}^{p^{n-1}} Q_i$$

If the number of partition intervals increases, the MLA mapping with respect to Q becomes the union of LA mapping with respect to the subdomains Q_i. That is, if $p \to \infty$, then

$$\begin{aligned}\text{MLA}(Q) &= \lim_{p\to\infty} \bigcup_{i=1}^{p^{n-1}} \text{conv}\{\text{MLA}[\text{vert}(Q_i)]\} \\ &= \lim_{p\to\infty} \bigcup_{i=1}^{p^{n-1}} \text{conv}\{\text{LA}[\text{vert}(Q_i)]\}\end{aligned} \tag{6}$$

Therefore, the image of MLA mapping of domain Q can be obtained approximately using the union of the images of LA mapping of its subdomains.

Check of Zero Inclusion Condition for the Existence of Multilinear Dependence

For $K = K^*$ and $s = s^*$, the characteristic polynomial $f(q) = \Delta(s^*, q, K^*)$ becomes a MLA mapping. Corollary 1 gives an effective method for checking the ZIC where the coefficients of characteristic polynomial are linear affine functions of physical parameters.

Following Eq. (6), the area of the image of MLA mapping can be expressed as follows:

$$\text{area}[\text{MLA}(Q)] = \lim_{p\to\infty} \text{area}\left(\bigcup_{i=1}^{p^{n-1}} \text{conv}\{\text{LA}[\text{vert}(Q_i)]\}\right) \tag{7}$$

If the right-hand term converges to an acceptable tolerance for some p, say $\bar{p}$, then

$$\text{area}[\text{MLA}(Q)] \approx \text{area}\left(\sum_{i=1}^{\bar{p}^{n-1}} \text{conv}\{\text{LA}[\text{vert}(Q_i)]\}\right) \tag{8}$$

The calculation procedure for the area of the image of the MLA mapping is stated as follows.

1) Calculate the area of conv{LA[vert(Q)]} as the initial value of area[MLA(Q)] denoted as area_{old} and set $p = 2$.

2) Partition the domain Q into p^{n-1} subdomains, denoted as Q_i, $i = 1, \ldots, p^{n-1}$, by partitioning q_j, $j \neq k$.

3) Calculate the size of

$$\text{area}\left(\bigcup_{i=1}^{p^{n-1}} \text{conv}\{\text{LA}[\text{vert}(Q_i)]\}\right)$$

as the new size of area[MLA(Q)] denoted as area_{new}.

Received March 6, 1992; revision received Nov. 15, 1992; accepted for publication Jan. 29, 1993.

*Postgraduate Student, Department of Mechanical Engineering.
†Associate Professor, Institute of Aeronautics and Astronautics.